Thanh Tien Nguyen
Faculty of Surveying, Mapping and Geographic Information, Hanoi University of Natural Resources and Environment, Vietnam
*** Corresponding author:** tdgis_ntthanh@163.com

FRACTIONAL VEGETATION COVER CHANGE DETECTION IN MEGACITIES USING LANDSAT TIME-SERIES IMAGES: A CASE STUDY OF HANOI CITY (VIETNAM) DURING 1986-2019

ABSTRACT. The objective of the study is to assess changes of fractional vegetation cover (FVC) in Hanoi megacity in period of 33 years from 1986 to 2016 based on a two endmember spectral mixture analysis (SMA) model using multi-spectral and multi-temporal Landsat-5 TM and -8 OLI images. Landsat TM/OLI images were first radiometrically corrected. FVC was then estimated by means of a combination of Normalized Difference Vegetation Index (NDVI) and classification method. The estimated FVC results were validated using the field survey data. The assessment of FVC changes was finally carried out using spatial analysis in GIS. A case study from Hanoi city shows that: (i) the proposed approach performed well in estimating the FVC retrieved from the Landsat-8 OLI data and had good consistency with in situ measurements with the statistically achieved root mean square error (RMSE) of 0.02 (R^2=0.935); (ii) total FVC area of 321.6 km^2 (accounting for 9.61% of the total area) was slightly reduced in the center of the city, whereas, FVC increased markedly with an area of 1163.6 km^2 (accounting for 34.78% of the total area) in suburban and rural areas. The results from this study demonstrate the combination of NDVI and classification method using Landsat images are promising for assessing FVC change in megacities.

KEY WORDS: Fractional vegetation cover; Landsat images; Change assessment; Megacities; Hanoi, Vietnam

CITATION: Thanh Tien Nguyen (2019) Fractional Vegetation Cover Change Detection In Megacities Using Landsat Time-Series Images: A Case Study Of Hanoi City (Vietnam) During 1986-2019. Geography, Environment, Sustainability, Vol.12, No 4, p. 175-187
DOI-10.24057/2071-9388-2019-112

INTRODUCTION

Vegetation is a general term for the plant community on the ground surface, such as forests, shrubs, grassland and agricultural crops, and it can intercept rainfall, alleviate runoffs, prevent desertification and conserve soil and water (Zhang et al. 2013a). Vegetation plays an important role in the exchanges of carbon, water, and energy at the land surface (Hoffmann and Jackson 2000). Fractional vegetation cover (FVC) refers to the percentage taken by the vertical projected area of vegetation (including leafs, stem and branches) in the total statistical area (Godínez-Alvarez et

al. 2009; Jing et al. 2011). FVC is not only one of the main biophysical parameters involved in the surface processes, which is also a necessary requirement for Numerical Weather Prediction, regional and global climate modelling, and global change monitoring (Avissar and Pielke 1989; Trimble 1990), but also an important parameter for describing the surface vegetation, a comprehensive quantitative variable for plant community on ground surface, and a basic data for characterizing ecosystems, playing an extremely crucial role in the study of regional ecosystems (Godínez-Alvarez et al. 2009; Jing et al. 2011). In addition, it can be also a key parameter in thermal remote sensing, since it is a basic parameter from which surface emissivities can be estimated (Jiménez-Muñoz et al. 2009). In terms of the state-of-art and development trend in the research on the FVC estimation, Zhang et al. (2013a) indicated the three main methods including: field measurement, remote sensing and a combination of the two. The former is a traditional method for the estimation of FVC, which includes visual estimation method, sampling method and instrument method according to different measuring modes (Zhang et al. 2013a) and plays an major role in survey of land surface vegetation. With the help of a digital camera and image processing software packages (e.g. Photoshop and ERDAS Imagine), Zhou and Robson (2001) estimated FVC faster and more accurate. However, the main advantage of these methods is that measurement is nearly impossible to gather enough data over a large area (Zhang et al. 2013a). The occurrences of remotely sensed imageries overcome most of these limitations of conventional methods. Remote sensing can be considered as an effective tool for observing the distribution and evolution of the FVC. The characteristics of large scale and periodic detection with remote sensing data make it possible to obtain vegetation coverage and its dynamic change in a large area (Chen et al. 2010; Xing et al. 2009). Particularly, since remotely sensed imageries of high spatial resolution satellite sensors such as Landsat Thematic Mapper (TM), Enhanced Thematic Mapper Plus (ETM+) and most recently the Operational Land Imager (OLI) started to become available, the FVC estimation and monitoring from space became easier (Alejandro and Omasa 2007; Zhang et al. 2013b). Several methods for the FVC estimation from remotely sensed data have been developed, and the main ones include empirical model (Zhou and Robson 2001), vegetation index (Choudhury 1987), sub-pixel unmixing models (Asner and Heidebrecht 2002) and linear spectral mixture models (Li 2003; Li 2008; Wu and Peng 2010). When comparing these methods, Zhang et al. (2013a) indicated that the shortcoming of the empirical model is the rely on in situ measurement data in specific regions, and the measured result is fairly accurate only if the study area is small. Whereas, the vegetation index method may be less accurate than the empirical model in estimating the FVC in certain localities. In addition, an accurate conversion relationship between vegetation index and the FVC is usually difficult to obtain (Zhang et al. 2013a). The linear mixed model combining four bands was more effective than the simple vegetation index in estimating the FVC. Particularly, for Landsat data, a maximum of four endmembers are usually used because the three visible bands are strongly correlated with each other (Small 2001; Theseira et al. 2002). The term endmember has been used by Xiao and Moody (2005) to refer to a pure surface material or land-cover type that is assumed to have a unique spectral signature. However, when applying this approach, Zhang et al. (2013a) indicated the serious weakness is the correct identification of $NDVI_{soil}$ and $NDVI_{veg}$ values. It is therefore, in this study, a method based on a combination of NDVI and classification method is proposed to identify these $NDVI_{soil}$ and $NDVI_{veg}$ values. In this method, NDVI provides a measure of vegetation density, whereas, the classification method classifies land cover into various types. Additionally, this study attempts to discuss how FVC changes in megacities are detected through Landsat images using the two endmember SMA model. At the same time, an assessment is conducted concerning the usability of the proposed method in vegetation monitoring.

MATERIALS AND METHODS

STUDY AREA

The city of Hanoi (latitudinally from 20°35'28.2"N to 21°24'15"N and longitudinally from 105°18'28.21"E to 106°02'15"E), the capital of Socialist Republic of Vietnam is the political, economic, cultural, scientific and technological center of the whole country. It is located in the center of the Northern Delta, northern Vietnam (Fig. 1.). After the new economic policies were approved in 1986, the Communist Party and national and municipal governments attracted international investments for urban development projects in Hanoi (Logan 2005). Particularly, Hatay province, Vinhphuc province's Melinh district and 4 communes of Hoabinh province's Luongson district were merged into the metropolitan area of Hanoi from August 2008 (Hiep 2014). Rapid urban development displaced vegetation in many areas in central Hanoi. Covering an area of 3,328.9 square kilometers, Hanoi is now the largest city in Vietnam by area. With an estimated population of 8.05 million and a population density of 2,300 people for every square kilometer in 2019, Hanoi satisfies criteria of being a megacity. It is therefore Hanoi is selected for this study, exhibiting rapid population growth and urban expansion in the form of encroachment to the limited agricultural areas in limited directions at the cost of destruction of vegetation coverage. The study of FVC changes plays an important role in integration of knowledge in decision-making process for future development of the city.

MATERIALS

In this study, a total of four daytime Landsat-5 TM and Landsat-8 OLI scenes acquired in July 1986 and June 2019 with 30-m spatial resolution were collected (Tab. 1.). All the daytime Landsat TM/OLI datasets were the standard terrain correction (L1TP) products, downloaded from the U.S. Geological Survey (USGS) website, which provides systematic radiometric and geometric accuracy estimates by incorporating ground control points (GCPs) from the global land survey of 2000 (GLS2000) and employing a digital elevation model (DEM) for topographic accuracy. DEM sources include the Shuttle Radar Topography Mission (SRTM), the National Elevation Dataset (NED), Canadian Digital Elevation Data (CDED), Digital Terrain Elevation Data (DTED), and GTOPO 30 (a global DEM from the USGS). All the datasets were projected in the UTM Zone N48 and WGS 1984 ellipsoid datum. In addition, the field survey data were also collected and used to validate FVC estimated from 2019 June Landsat image.

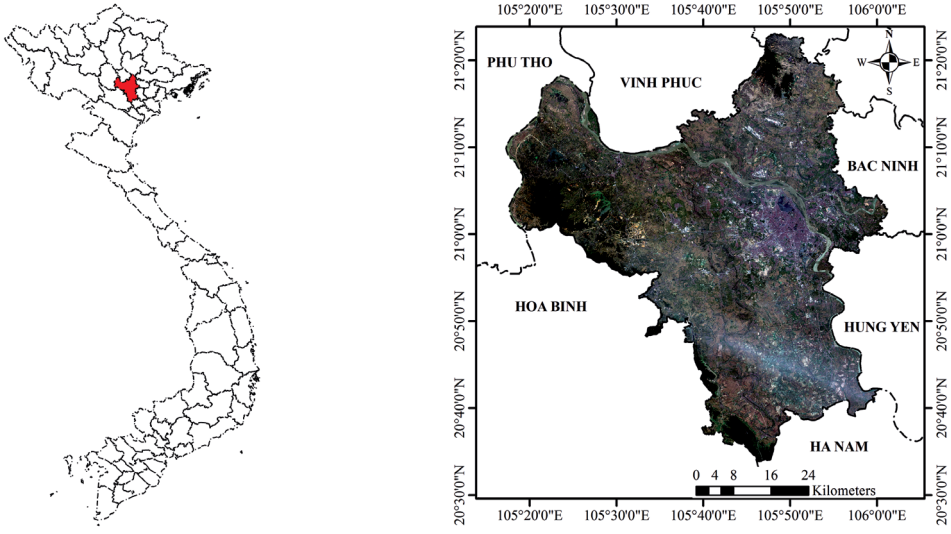

Fig. 1. A true color RGB composite from Landsat-8 OLI image collected on June 26, 2019 in Hanoi city (right), northern Vietnam (left)

Table 1. Details of the Landsat datasets used for FVC change detection in Hanoi city

Landsat sensors	Path/row	Acquisition date (yy-mm-dd)	Acquisition time (hh:mm:ss)	Spatial resolution (m)	Image quality
TM	127/045	01-7-1986	02:46:39	30	9/9
TM	127/046	01-7-1986	02:47:03	30	9/9
OLI	127/045	26-6-2019	03:23:18	30	9/9
OLI	127/046	26-6-2019	03:23:42	30	9/9

METHODS

Image pre-processing

This process involved two steps. The Landsat instruments have aged, and their characteristics have changed since launch (Chander and Markham 2003), therefore, the first step of this process involved the conversion of calibrated digital numbers (Q_{cal}) to top of atmosphere radiance ($L_{at-sensor,\lambda}$) using inflight sensor calibration parameters. The equation (1) and (2) are used to perform the (Q_{cal})-to-$L_{at-sensor,\lambda}$) conversion for Landsat-5 TM (Chander et al. 2009; Vu and Nguyen 2018a) and Landsat-8 OLI data (Nguyen and Vu 2019; Vu and Nguyen 2018b; Zanter 2015), respectively:

$$L_\lambda = \left(\frac{L\max_\lambda - L\min_\lambda}{Q_{cal\_\max} - Q_{cal\_\min}}\right) \times (Q_{cal} - Q_{cal\_\min}) + L\min_\lambda \quad (1)$$

where: L_λ is spectral radiance at the sensor's aperture [W/m^2.sr.µm]; Q_{cal} is quantized calibrated pixel values (DN values); Q_{cal_min} and Q_{cal_max} are minimum quantized calibrated pixel values corresponding to $L_{min\lambda}$ and $L_{min\lambda}$ respectively; $L_{min\lambda}$ and $L_{max\lambda}$ are spectral at-sensor radiance, scaled to and respectively [W/m^2.sr.µm].

$$L_{at-sensor,\lambda} = M_L Q_{cal} + \Delta_L \quad (2)$$

where: $L_{at-sensor,\lambda}$ is the at-sensor radiance or Top of Atmospheric (TOA) radiance [W/(m^2·sr·µm)] at the wavelength λ (µm); M_L is the radiance multiplicative scaling factor for the band (RADIANCE_MULT_BAND_n from the metadata); Q_{cal} is the the quantized calibrated pixel value; Δ_L is the radiance additive scaling factor for the band (RADIANCE_ADD_BAND_n from the metadata)

The second step involves compensating for atmospheric effects for Landsat reflective bands using FLAASH algorithm developed by the Air Force Phillips Laboratory, Hanscom AFB and Spectral Sciences, Inc (SSI) (Adler-Golden et al. 1999). The spectral radiance is calculated using equation (3) (Adler-Golden et al. 1998; Adler-Golden et al. 1999):

$$L^* = \left(\frac{Ap}{1 - p_e S}\right) + \left(\frac{Bp_e}{1 - p_e S}\right) + L_a^* \quad (3)$$

where: ρ is the pixel surface reflectance; ρ_e is an average surface reflectance for the pixel and a surrounding region; S is the spherical albedo of the atmosphere; L_a^* is the radiance back scattered by the atmosphere; A and B are coefficients that depend on atmospheric and geometric conditions but not on the surface.

The values of A, B, S and L_a^* are determined from MODTRAN4 calculations that use the viewing and solar angles and the mean surface elevation of 10m. These atmospheric characteristics quantities assume a certain model atmosphere, urban aerosol type, and initial visible range of 40km. All of the Landsat sensors do not have the appropriate bands to perform the water retrieval (Flaash 2009). Therefore, in this study, the water retrieval was performed using a constant column water vapor amount for all pixels in the image which is determined according to the standard column water vapor amount for the tropical atmosphere model. After the water retrieval is performed, the spatially averaged reflectance ρ_e is estimated using equation (4) (Adler-Golden et al. 1998; Adler-Golden et al. 1999):

$$L_e = \left(\frac{(A+B)p_e}{1-p_eS}\right) + L_a^* \quad (4)$$

The FLAASH model includes a method for retrieving an estimated aerosol/haze amount from selected dark land pixels in the scene. The method is based on observations by Kaufman et al. (1997) of a nearly fixed ratio between the reflectances for such pixels at 660 nm and 2100 nm.

Estimation of fractional vegetation cover

The form of the linear spectral mixture analysis is (Jiménez-Muñoz et al. 2009; Li 2003; Small 2001):

$$R_k = \sum_{i=1}^{n} f_i r_{i,k} + e_k \quad (5)$$

where: R_k is the reflectance for each band (k), n is the number of endmembers in a pixel, f_i is the fraction of endmember i, $r_{i,k}$ is the reflectance of endmember i at band k, and e_k is the residual term at band k.

The derived fractions of endmembers are often subject to the unity constraint:

$$\sum_{i=1}^{n} f_i = 1 \quad (6)$$

Deardorff (1978) expressed heat and moisture coefficients as linear functions of fractional vegetation cover. The general form of the linear relation is written as:

$$\Phi = (1-\sigma) \times \Phi_{\sigma=0} + \sigma \times \Phi_{\sigma=1} \quad (7)$$

where: Φ is the heat or moisture coefficient, $\Phi_{\sigma=0}$ and $\Phi_{\sigma=1}$ are contributions from vegetated ground and bare soil, respectively, and σ is fractional vegetation cover. Wittich and Hansing (1995) applied this general formulation to NDVI for the approximation of FVC using the two endmember SMA model:

$$NDVI = f^* NDVI_{veg} + (1-f)^* NDVI_{soil} \quad (8)$$

which can be rewritten as:

$$f = \frac{NDVI - NDVI_{soil}}{NDVI_{veg} - NDVI_{soil}} \quad (9)$$

where: $NDVI_{veg}$ is the NDVI value of a pure green vegetation pixel, $NDVI_{soil}$ is the NDVI of bare soil, NDVI is the value of NDVI, given by:

$$NDVI = \frac{\rho_{nir} - \rho_{red}}{\rho_{nir} - \rho_{red}} \quad (10)$$

where: ρ_{nir} and ρ_{red} are the at-surface reflectivities obtained from sensor bands located in the near infrared (NIR) and red spectral regions.

The main problem when applying equation (7) is the correct identification of $NDVI_{soil}$ and $NDVI_{veg}$ values. This is a critical task, so these values are region- and season-specific. Hence, for global studies with very low spatial resolution data (0.15º x 0.15º), Gutman and Ignatov (1998) proposed $NDVI_{soil}$=0.04 ± 0.03 and $NDVI_{veg}$=0.52 ± 0.03, which correspond to minimum and maximum values of the desert and evergreen clusters, respectively. Sobrino and Raissouni (2000) considered a similar value for $NDVI_{veg}$ (0.5), but a $NDVI_{soil}$ value of 0.2. In this study, the land surface coverage was mainly composed of vegetation, residential area, surface water (rivers, lakes and small ponds), bare soil and sand. To accurately estimate $NDVI_{veg}$ and $NDVI_{soil}$, the land cover in the study area was first classified into five categories of vegetation, residential area, surface water (rivers, lakes and small ponds), bare soil and sand on a Supervised Maximum Likelihood (ML) Classification method, which calculated the discriminant functions for each pixel in the image (Richards and Richards 1999). The 5% and 95% confidence levels of NDVI values corresponding to each land cover type, $NDVI_{5\%}$ and $NDVI_{95\%}$, were then computed. $NDVI_{soil}$ and $NDVI_{veg}$ of each pixel were then calculated for each image using the following equations:

$$NDVI_{soil} = \sum_{i}^{n} NDVI_{5\%}{}^* P_i \quad (11)$$

$$NDVI_{veg} = \sum_{i}^{n} NDVI_{95\%}{}^* P_i \quad (12)$$

where: P_i is the pixel values in the i^{th} binary images with 0 and 1 representing none and one of the above classified land cover type pixels, respectively; n is the number of land cover types.

Fractional vegetation cover change detection

The change of FVC at pixel i is computed using the following equation:

$$f_{change\_1} = f_{time\_2i} - f_{time\_1i} \quad (13)$$

where: f_{time_1i} and f_{time_2i} are FVC of the i^{th} pixel estimated in the first and second year. In this study, five levels of FVC changes are obtained and were ranked accordingly: (i) high decrease, if $-1 \leq f_{change} \leq -0.6$; (ii) low decrease, if $-0.6 < f_{change} \leq -0.2$; (iii) no change, if $-0.2 < f_{change} \leq 0.2$; (iv) low increase, $0.2 < f_{change} \leq 0.6$ and (v) high increase, if $0.6 < f_{change} \leq 1.0$.

RESULTS AND DISCUSSIONS

Accuracy assessment

In this study, in order to assess the accuracy of the Landsat-8 OLI data in FVC estimation, a validation of ground quadratic data and the FVC results retrieved from the Landsat-8 OLI data was made. A total of 32 in situ measurements in forest, grassland, farming land, building and surface water were used to do the fitting analysis for accuracy assessment. Data from Fig. 2 shows the result of validation of the FVC as retrieved from the Landsat-8 OLI against the 32 in situ measurements. Obviously the FVC retrieved from the June 2019 Landsat-8 OLI data fits well with the field survey results. The root mean square error (RMSE) of the FVC values retrieved from June 2019 Landsat-8 OLI with reference to the in situ data is 0.02 with R square = 0.935. Data in Figure 2 shows that there are 2 points in the upper right corner which are located quite far away from the regression line and can be considered outliers. The measured and estimated FVC values of these points were [0.98; 0.79] and [0.7; 1.0], respectively. The value difference of the first pair shows that there was not much difference between measured and estimated FVC of 0.19 in this area. The second pair had a bigger difference in value of 0.3. Uncertainties may have affected the accuracy of the proposed method. The main uncertainty was the inconsistencies in the spatial resolution between in situ samples of (40 m × 40 m for a large area; 30 m × 30 m for a small area) and Landsat TM/OLI images (30 m × 30 m). In addition, the effects of leaf area index under different vegetation types and land cover types were also not taken into consideration in the FVC estimation. These uncertainties may have caused the fractional vegetation cover estimation results to have the above-mentioned outliers. However, these outliers only account for 6.2% of total in situ samples (2/32). More importantly, a low value of RMSE of 0.02 and a relatively high R squared (R^2 = 0.935) indicate the reliability of the predicted model. The results show that the proposed approach performed well in estimating FVC and had good consistency with in situ measurements.

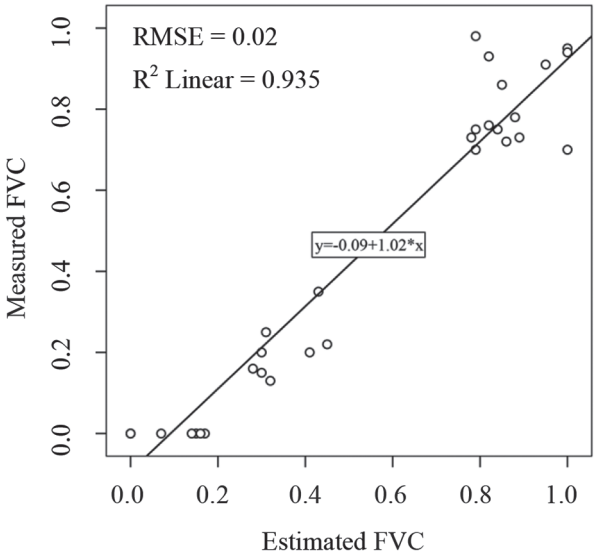

Fig. 2. Scatter plot of measured FVC and FVC estimated from Landsat imagery

Fractional vegetation cover

The FVC determined from Landsat TM and OLI images is shown in Fig. 3 and 4. Data in Fig. 3 shows that, in general, the FVC obtained in 2019 was higher than that of 1986, especially in suburban areas. Data from histograms in Fig. 4 shows that, when comparing to the FVC in 2019, the total area of low FVC (approximately 0) in 1986 accounts for larger area. Meanwhile the FVC ranging from 0.4 to 0.8 in 2019 had more area than that of 1986. Data from the histogram in Fig. 4. (left) and Tab. 2. obtained in 1996 demonstrates that the largest area of 964.4 km^2 was detected with low-density vegetation cover (0.2<FVC≤0.4) which accounting for 28.8% of the total area, followed by 825.0 km^2 (24.7%) of very low-density vegetation cover (0.0<FVC≤0.2), 678.8 km^2 (16.2%) of medium-density vegetation cover (0.4<FVC≤0.6), 542.0 km^2 (20.3%) of high-density vegetation cover (0.6<FVC≤0.8), and 335.5 km^2 (10.0%) of very high-density vegetation cover (0.8<FVC≤1.0). The density line in Fig. 4. (left) shows a fairly uniform distribution among FVC intervals. The bell-shaped curve at about 0.3 indicates that the FVC in the range of from 0.2 to 0.3 takes up a larger area than the other intervals. Meanwhile, data from the histogram in Fig. 4. (right) and Tab. 2. obtained in 2019 demonstrates that the FVC area in the range of 0.0 to 0.2 had decreased to 229 km^2 (accounting for only 6.8% of the study area), low-density vegetation cover (0.2<FVC≤0.4) accounted for 616.2 km^2 (18.4%), medium-density vegetation cover (0.4<FVC≤0.6) accounted for a larger area of 1277.9 km^2

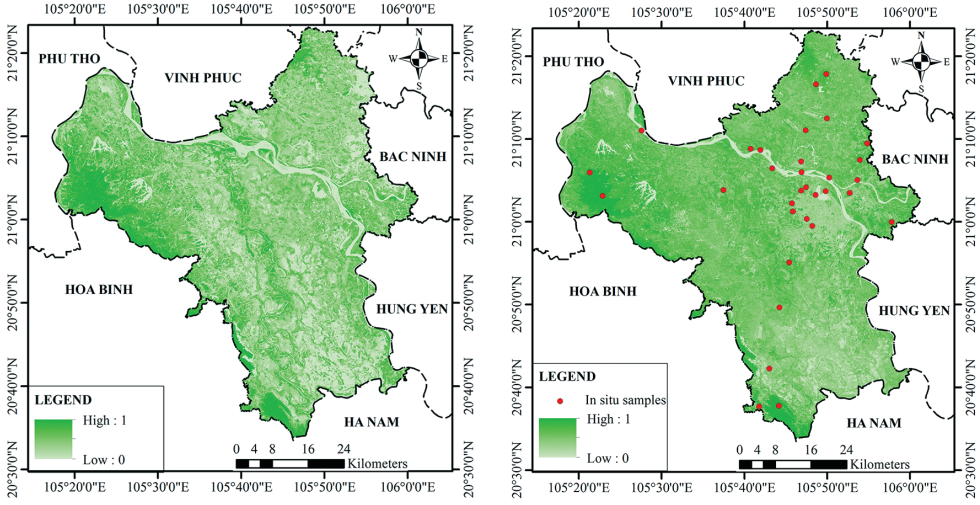

Fig. 3. Maps of FVC estimated from Landsat-5 TM images in 1986 (left) and Landsat-8 OLI images in 2019 (right) in Hanoi, Vietnam

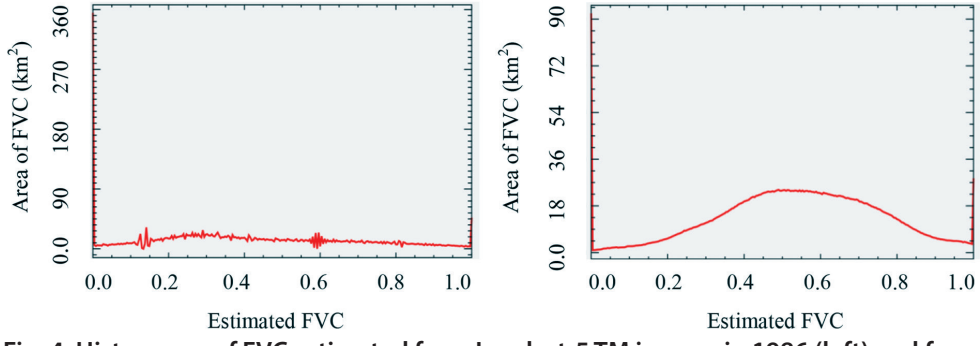

Fig. 4. Histograms of FVC estimated from Landsat-5 TM images in 1986 (left) and from Landsat-8 OLI images in 2019 (right) in Hanoi, Vietnam

Table 2. Summary of FVC areas in 1986 and 2019 in Hanoi, Vietnam

FVC	Levels	1986		2019	
		Area (km^2)	Percentage (%)	Area (km^2)	Percentage (%)
[0.0, 0.2]	Very low	825.0	24.7	229.0	6.8
[0.2, 0.4]	Low	964.4	28.8	616.2	18.4
[0.4, 0.6]	Medium	678.8	20.3	1277.9	38.2
[0.6, 0.8]	High	542.0	16.2	982.4	29.4
[0.8, 1.0]	Very high	335.5	10.0	240.1	7.2
Total		3345.7	100.0	3345.7	100.0

(38.2%), high-density vegetation cover (0.6<FVC≤0.8) with 982.4 km^2 (29.4%), and very high-density vegetation cover (0.8<FVC ≤1.0) with only 240.1 km^2 (7.2%). The density line in Fig. 4. (right) shows the bell-shaped curve was at in the range of 0.4-0.6 and 0.6-0.8 indicating that the FVC areas distributed mainly in the range of 0.4 to 0.8.

Fractional vegetation cover changes

The results of FVC changes during the period of from 1986 to 2019 in the area of Hanoi are shown in Fig. 5 and 6, and are statistically summarized in Tab. 3. Data from Tab. 3 demonstrates that FVC has been significantly reduced to an insignificant area of 0.9 km^2 (accounting for 0.03% of the Hanoi surface area) mainly occurring in the city center (Fig. 5). FVC slightly reduced an area of 321.6 km^2 (accounting for 9.61% of the total area). These areas were mainly detected in densely populated areas in the center of the city. No change of FVC covered an area of 1724.8 km^2 (accounting for 51.55%). Data from the histogram in Fig. 6 also shows that FVC change peaks at about 0.0 which occupies a very large area of 126 km^2 (3.8% of total area). This indicates the vegetation density in these areas remained unchanged after 33 years. Meanwhile, FVC in the range of from 0.2 to 0.6 had increased markedly with an area of 1163.6 km^2 (accounting for 34.78% of the total area). In addition, some areas of FVC high increase were also detected with an area of 134.8 km^2 (equivalent to 4.03% of the total area). It can be seen that FVC in the Hanoi city increased mainly in suburban districts and strongly decreased in urban districts in period of 33 years from 1986 to 2019.

The results showed that fractional vegetation cover has dramatically decreased in urban districts such as Tayho, Badinh, Caugiay, Dongda, Hoankiem, Thanhxuan, Haibatrung, Hoangmai and Longbien and some areas of Donganh suburban district because of the incessant urbanization process in the central urban areas and some sub-urban areas of the Hanoi city, especially after the Doi Moi Policy started in 1986 (Logan 2005) which has greatly contributed to the rapid urbanization process in Hanoi city (Tsunoda et al. 2014). The rapid development in these urban areas has brought the replacement of among land cover types especially vegetation cover replaced with urban built-up land (Nguyen et al. 2019). These findings were similar to those reported in previous studies (Hoang 2016; Hoang 2017). Particularly, the emergence of Hatay province, Vinhphuc province's Melinh district and 4 communes of Hoabinh province's Luongson district into the metropolitan area of Hanoi in August 2008 (Hiep 2014) has led the rapid urban development displaced vegetation in many areas, especially in urban districts. The increase of FVC was mainly detected in sub-urban districts such as Socson,

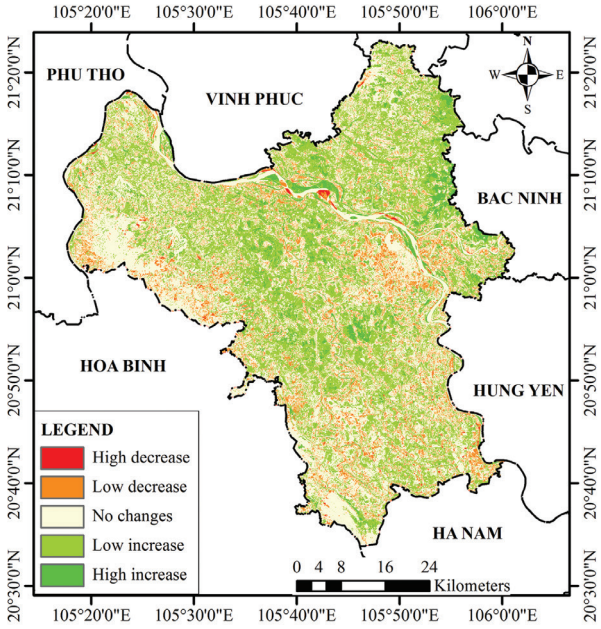

Fig. 5. Map of FVC changes in Hanoi city from 1986 to 2019

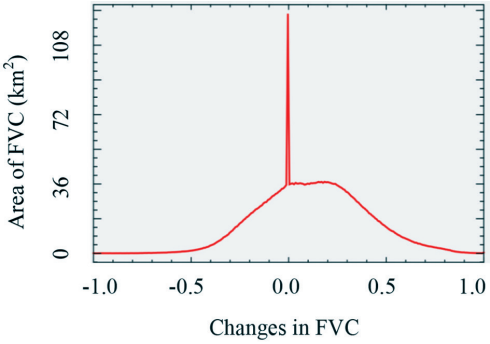

Fig. 6. Histograms of FVC estimated from Landsat-5 TM images in 1986 (left) and from Landsat-8 OLI images in 2019 (right) in Hanoi, Vietnam

Myduc, Sontay, Chuongmy, Quocoai, Thachthat and Bavi. This increase of FVC was mainly due to afforestation policies to increase the forest cover in Bavi National Park (Thinh 2006) and forests in these sub-urban districts (Clement and Amezaga 2009; Clement et al. 2009).

CONCLUSIONS

In this study, fractional vegetation cover changes in Hanoi city (Vietnam) during the period of 1986-2019 were assessed using the two endmember spectral mixture analysis model which is based on the combination of NDVI and classification method from Landsat-5 TM and -8 OLI images. Landsat remotely sensed images were first pre-processed. FVC was then estimated by NDVI and Maximum likelihood (ML) classification algorithm. The estimated FVC results were validated using 32 in situ measurements. The assessment of FVC changes was finally carried out with the help of GIS. It was found that the combination of NDVI and ML method allows for an improved estimation of FVC with the statistically achieved root mean square error (RMSE) of 0.02 (R^2=0.935). Total FVC area of 321.6 km^2

Table 3. Summary of the FVC changes in Hanoi city from 1986 to 2019

FVC change	Levels of change	Area (km^2)	Percentage (%)	Zones
[-1.0; -0.6]	High decrease	0.9	0.03	Small areas of urban districts such as Tayho and Donganh.
[-0.6; -0.2]	Low decrease	321.6	9.61	Some areas of urban districts: Tayho, Badinh, Caugiay, Dongda, Hoankiem, Thanhxuan, Haibatrung, Hoangmai and Longbien.
[-0.2; 0.2]	No change	1724.8	51.55	Areas of sub-urban districts such as Bavi, Myduc, Sontay and of urban district such as Tayho, Badinh, Hoankiem, and Haibatrung.
[0.2; 0.6]	Low increase	1163.6	34.78	Outer-city districts such as Socson, Myduc, Sontay, Chuongmy, Quocoai, Thachthat and Bavi.
[0.6; 1.0]	High increase	134.8	4.03	Outer-city districts such as east of Dong Anh, north of Gialam and Thanhoai, north of Danphuong and south of Melinh.
Total		3345.7	100.0	

(accounting for 9.61% of the total area) was reduced in the center of the city, whereas, FVC increased markedly with an area of 1163.6 km^2 (accounting for 34.78% of the total area) in suburban and rural areas. The results from this study support the combination of NDVI and ML classification method from Landsat images in FVC change detection in megacities.

REFERENCES

Adler-Golden S. et al. (1999). FLAASH, a MODTRAN4 atmospheric correction package for hyperspectral data retrievals and simulations. In: Proc. 7th Ann. JPL Airborne Earth Science Workshop, 1998. JPL Publication Pasadena, CA, 9-14.

Adler-Golden S.M. et al. (1999). Atmospheric correction for shortwave spectral imagery based on MODTRAN4. In: Imaging Spectrometry V, 1999. International Society for Optics and Photonics, 61-70. http://dx.doi.org/10.1117/12.366315

Alejandro M., Omasa K. (2007). Estimation of vegetation parameter for modeling soil erosion using linear Spectral Mixture Analysis of Landsat ETM data ISPRS Journal of Photogrammetry and Remote Sensing 62. 309-324.

Asner G.P., Heidebrecht K.B. (2002). Spectral unmixing of vegetation, soil and dry carbon cover in arid regions: comparing multispectral and hyperspectral observations International Journal of Remote Sensing, 23, 3939-3958.

Avissar R., Pielke R.A. (1989). A parameterization of heterogeneous land surfaces for atmospheric numerical models and its impact on regional meteorology Monthly Weather Review, 117, 2113-2136.

Chander G., Markham B. (2003). Revised Landsat-5 TM radiometric calibration procedures and postcalibration dynamic ranges IEEE Transactions on geoscience and remote sensing, 41, 2674-2677.

Chander G., Markham B.L., Helder D.L. (2009). Summary of current radiometric calibration coefficients for Landsat MSS, TM, ETM+, and EO-1 ALI sensors Remote sensing of environment, 113, 893-903. https://dx.doi.org/10.1016/j.rse.2009.01.007

Chen F., Qiu Q, Xiong Y., Huang S. (2010). Pixel unmixing based on linear spectral mixture model: methods and comparison Remote Sens Info, 4, 22-28.

Choudhury B.J. (1987). Relationships between vegetation indices, radiation absorption, and net photosynthesis evaluated by a sensitivity analysis Remote Sensing of Environment, 22, 209-233.

Clement F., Amezaga JM (2009). Afforestation and forestry land allocation in northern Vietnam: analysing the gap between policy intentions and outcomes Land Use Policy, 26, 458-470.

Clement F., Orange D., Williams M., Mulley C., Epprecht M. (2009). Drivers of afforestation in Northern Vietnam: assessing local variations using geographically weighted regression Applied Geography, 29, 561-576.

Deardorff J.W. (1978). Efficient prediction of ground surface temperature and moisture, with inclusion of a layer of vegetation Journal of Geophysical Research: Oceans, 83, 1889-1903.

Flaash Us.G. (2009). Atmospheric Correction Module: QUAC and Flaash User Guide v. 4.7 ITT Visual Information Solutions Inc: Boulder, CO, USA.

Godínez-Alvarez H., Herrick J., Mattocks M., Toledo D., Van Zee J. (2009). Comparison of three vegetation monitoring methods: their relative utility for ecological assessment and monitoring Ecological indicators, 9, 1001-1008.

Gutman G., Ignatov A. (1998). The derivation of the green vegetation fraction from NOAA/AVHRR data for use in numerical weather prediction models International Journal of remote sensing, 19, 1533-1543.

Hiep N.T. (2014). Economic Evaluation of Transportation Infrastructure Science, 47, 415-455.

Hoang A.H. (2016). Fractional Vegetation Cover Estimation in Urban Area of Hanoi City using Landsat 8 OLI Images VNU Journal of Science: Earth and Environmental Sciences, 32, 8.

Hoang A.H. (2017). Assessment of Fractional Vegetation Cover Changes in some Urban and Sub-urban Areas of Hanoi Using Multi-spectral and Multi-temporal LANDSAT Images VNU Journal of Science: Earth and Environmental Sciences, 33, 8.

Hoffmann W.A., Jackson R.B. (2000) Vegetation–climate feedbacks in the conversion of tropical savanna to grassland Journal of Climate, 13, 1593-1602.

Jiménez-Muñoz J., Sobrino J., Plaza A., Guanter L., Moreno J., Martínez P. (2009). Comparison between fractional vegetation cover retrievals from vegetation indices and spectral mixture analysis: Case study of PROBA/CHRIS data over an agricultural area Sensors, 9, 768-793.

Jing X., Yao W-Q., Wang J-H., Song X-Y. (2011). A study on the relationship between dynamic change of vegetation coverage and precipitation in Beijing's mountainous areas during the last 20 years Mathematical and Computer Modelling, 54, 1079-1085.

Kaufman Y., Wald A., Remer L., Gao B., Li R., Flynn L. (1997). Remote sensing of aerosol over the continents with the aid of a 2.2 m channel IEEE Trans Geosci Remote Sens, 35, 1286-1298.

Li M. (2003). The method of vegetation fraction estimation by remote sensing Beijing: Chinese Academy of Sciences.

Li X. (2008). Quantitive retrieval of sparse vegetation cover in arid regions using hyperspectral data Beijing: Chinese Acanemy of Forestry.

Logan W.S. (2005). The cultural role of capital cities: Hanoi and Hue, Vietnam Pacific Affairs, 78, 559-575.

Nguyen T.M., Lin T-H., Chan H-P. (2019). The Environmental Effects of Urban Development in Hanoi, Vietnam from Satellite and Meteorological Observations from 1999–2016 Sustainability 11, 1768.

Nguyen T.T., Vu T.D. (2019). Use of Hot Spot Analysis to Detect Underground Coal Fires from Landsat-8 TIRS Data: A Case Study in the Khanh Hoa Coal Field, North-East of Vietnam Environment and Natural Resources Journal, 17, 1-10; DOI: 10.32526/ennrj. 32517.32523. 32019.32517.

Richards J.A., Richards J. (1999). Remote sensing digital image analysis - An Introduction vol 3. Springer, Berlin, Heidelberg

Small C. (2001). Estimation of urban vegetation abundance by spectral mixture analysis International journal of remote sensing 22, 1305-1334.

Sobrino J., Raissouni N. (2000). Toward remote sensing methods for land cover dynamic monitoring: Application to Morocco International journal of remote sensing 21, 353-366.

Theseira M., Thomas G., Sannier C. (2002). An evaluation of spectral mixture modelling applied to a semi-arid environment International Journal of Remote Sensing, 23, 687-700.

Thinh V.T. (2006). Bird species richness and diversity in relation to vegetation in Bavi National Park, Vietnam Ornithological Science, 5, 121-125.

Trimble S. (1990). Geomorphic effects of vegetation cover and management: some time and space considerations in prediction of erosion and sediment yield Vegetation and erosion Processes and environments, 55-65.

Tsunoda T., Cuong T.C., Dong T.D., Yen N.T., Le N.H., Phong T.V., Minakawa N. (2014). Winter refuge for Aedes aegypti and Ae. albopictus mosquitoes in Hanoi during Winter PloS one 9:e95606.

Vu T.D., Nguyen T.T. (2018a). Remote Sensing and GIS-based River Bank Accretion/Erosion Assessment in the Confluence of Thao-Da-Lo Rivers, North East of Vietnam EnvironmentAsia 11.

Vu T.D., Nguyen T.T. (2018b). Spatio-temporal changes of underground coal fires during 2008–2016 in Khanh Hoa coal field (North-east of Viet Nam) using Landsat time-series data Journal of Mountain Science, 15, 2703-2720.

Wittich K., Hansing O. (1995). Area-averaged vegetative cover fraction estimated from satellite data International Journal of Biometeorology, 38, 209-215.

Wu J., Peng D-l. (2010). A research on extracting information of the arid regions' vegetation coverage using improved model of spectral mixture analysis. In: 2010 International Conference on Multimedia Technology, IEEE, 1-5.

Xiao J., Moody A. (2005). A comparison of methods for estimating fractional green vegetation cover within a desert-to-upland transition zone in central New Mexico, USA Remote sensing of environment, 98, 237-250.

Xing Z., Feng Y., Yang G., Wang P., Huang W-j. (2009). Method of estimating vegetation coverage based on remote sensing Remote Sens Tech Appl, 24, 849-854.

Zanter K. (2015). Landsat 8 (L8) data users handbook Survey, Department of the Interior US Geological.

Zhang X., Liao C., Li J., Sun Q. (2013a). Fractional vegetation cover estimation in arid and semi-arid environments using HJ-1 satellite hyperspectral data International Journal of Applied Earth Observation and Geoinformation, 21, 506-512.

Zhang Y., Odeh I.O., Ramadan E. (2013b). Assessment of land surface temperature in relation to landscape metrics and fractional vegetation cover in an urban/peri-urban region using Landsat data International Journal of Remote Sensing, 34, 168-189.

Zhou Q., Robson M. (2001). Automated rangeland vegetation cover and density estimation using ground digital images and a spectral-contextual classifier International Journal of Remote Sensing, 22, 3457-3470.

Received on August 17th, 2019 Accepted on November 07th, 2019